

## SPECTROSCOPY OF THE INNER COMPANION OF THE PULSAR PSR J0337+1715

DAVID L. KAPLAN<sup>1</sup>, MARTEN H. VAN KERKWIJK<sup>2</sup>, DETLEV KOESTER<sup>3</sup>, INGRID H. STAIRS<sup>4</sup>, SCOTT M. RANSOM<sup>5</sup>, ANNE M. ARCHIBALD<sup>6,7</sup>, JASON W. T. HESSELS<sup>6,8</sup>, JASON BOYLES<sup>9,10</sup>

*ApJL, in press*

### ABSTRACT

The hierarchical triple system PSR J0337+1715 offers an unprecedented laboratory to study secular evolution of interacting systems and to explore the complicated mass-transfer history that forms millisecond pulsars and helium-core white dwarfs. The latter in particular, however, requires knowledge of the properties of the individual components of the system. Here we present precise optical spectroscopy of the inner companion in the PSR J0337+1715 system. We confirm it as a hot, low-gravity DA white dwarf with  $T_{\text{eff}} = 15,800 \pm 100$  K and  $\log_{10}(g) = 5.82 \pm 0.05$ . We also measure an inner mass ratio of  $0.1364 \pm 0.0015$ , entirely consistent with that inferred from pulsar timing, and a systemic radial velocity of  $29.7 \pm 0.3$  km s<sup>-1</sup>. Combined with the mass ( $0.19751 M_{\odot}$ ) determined from pulsar timing, our measurement of the surface gravity implies a radius of  $0.091 \pm 0.005 R_{\odot}$ ; combined further with the effective temperature and extinction, the photometry implies a distance of  $1300 \pm 80$  pc. The high temperature of the companion is somewhat puzzling: with current models, it likely requires a recent period of unstable hydrogen burning, and suggests a surprisingly short lifetime for objects at this phase in their evolution. We discuss the implications of these measurements in the context of understanding the PSR J0337+1715 system, as well as of low-mass white dwarfs in general.

*Subject headings:* binaries: spectroscopic — pulsars: individual (PSR J0337+1715) — stars: atmospheres — stars: neutron — white dwarfs

### 1. INTRODUCTION

White dwarfs (WDs) are among the best-understood stars, enabling their use as astrophysical tools in investigations of, e.g., the ages and masses of astrophysical systems (e.g., Althaus et al. 2010). However, the lowest-mass WDs with He cores — Extremely-Low Mass (ELM) WDs with masses  $< 0.2 M_{\odot}$  (Kilic et al. 2012; Brown et al. 2013, and references therein) — still defy complete understanding, with few reliable independent measurements of masses, sizes and ages known (e.g., van Kerkwijk et al. 1996; Bedin et al. 2005).

Yet, these properties are important for understanding the evolution of ELM WDs and the binaries they are

found in (Iben & Livio 1993; Marsh, Dhillon, & Duck 1995). For instance, while one would naively expect low-mass WDs to cool quickly, given their relatively large size and small heat capacity, some ELM WDs can remain bright and hot (cf. Lorimer et al. 1995) because they have outer hydrogen layers sufficiently thick for nuclear fusion to continue — stably or otherwise — for several Gyr (Alberts et al. 1996; Serenelli et al. 2002; Panei et al. 2007; Althaus, Miller Bertolami, & Córscico 2013). Improving our understanding of ELM WD cooling would aid in evolutionary models for, e.g., millisecond pulsars and the later stages of mass transfer (e.g., Tauris et al. 2012; Antoniadis et al. 2012, 2013; Kaplan et al. 2013). Similarly, improved masses and radii would aid in determining the final fates of double-WD binaries (Deloye & Bildsten 2003; Marsh, Nelemans, & Steeghs 2004; D’Antona et al. 2006; Kaplan, Bildsten, & Steinfadt 2012): R CrB stars, AM CVn binaries, or even SNe Ia (Iben & Tutukov 1984; Webbink 1984).

PSR J0337+1715 (hereafter PSR J0337; Ransom et al. 2014) was discovered in the 350 MHz Green Bank Telescope Driftscan survey (Boyles et al. 2013; Lynch et al. 2013), and initial timing observations found a 2.7 ms spin period, a 1.6 d orbital period, and a likely companion mass of  $0.1\text{--}0.2 M_{\odot}$ , all of which are consistent with expectations for a fully-recycled pulsar with a low-mass He WD companion (van Kerkwijk et al. 2005; Tauris et al. 2012). However, further deviations to the observed spin period soon became apparent, suggesting the presence of an additional body in the system. This was confirmed with an intensive timing campaign, finding an outer orbital period of 327 d (Ransom et al. 2014). By comparing the pulsar’s pulse arrival times with numerical integrations of possible orbits, the masses, inclinations, and

<sup>1</sup> Department of Physics, University of Wisconsin-Milwaukee, 1900 E. Kenwood Boulevard, Milwaukee, WI 53211, USA; kaplan@uwm.edu

<sup>2</sup> Department of Astronomy and Astrophysics, University of Toronto, 50 St. George St., Toronto, ON, M5S 3H8, Canada; mhvk@astro.utoronto.ca

<sup>3</sup> Institut für Theoretische Physik und Astrophysik, University of Kiel, 24098 Kiel, Germany

<sup>4</sup> Department of Physics and Astronomy, University of British Columbia, 6224 Agricultural Road, Vancouver, British Columbia V6T 1Z1, Canada

<sup>5</sup> National Radio Astronomy Observatory, 520 Edgemont Road, Charlottesville, Virginia 22903-2475, USA

<sup>6</sup> ASTRON, the Netherlands Institute for Radio Astronomy, Postbus 2, 7990 AA, Dwingeloo, The Netherlands

<sup>7</sup> Department of Physics, McGill University, 3600 rue University, Montreal, Quebec H3A 2T8, Canada

<sup>8</sup> Astronomical Institute ‘Anton Pannekoek’, University of Amsterdam, Postbus 94249, 1090 GE Amsterdam, The Netherlands

<sup>9</sup> Department of Physics and Astronomy, West Virginia University, White Hall, Box 6315, Morgantown, West Virginia 26506-6315, USA

<sup>10</sup> Physics and Astronomy Department, Western Kentucky University, 1906 College Heights Boulevard #11077, Bowling Green, Kentucky 42101-1077, USA

orbital parameters of the system could be determined precisely (Ransom et al. 2014, Archibald et al. 2014, in prep.), with a pulsar mass of  $1.4378 \pm 0.0013 M_{\odot}$ , an inner companion mass of  $0.19751 \pm 0.0015 M_{\odot}$ , and an outer companion mass of  $0.4101 \pm 0.0003 M_{\odot}$ ; both inner and outer orbits are inclined by about  $39^{\circ}$  to the plane of the sky.

Before the nature of the system was fully determined, we identified an unusually blue object coincident with it, which, based on initial spectroscopy and photometry, we identified as the inner companion, almost certainly a hot low-mass WD (Ransom et al. 2014). The brightness of the system, its proximity, and the detailed constraints offered by pulsar timing make the system a fantastic laboratory to explore the atmosphere, structure, and evolution of ELM WDs. Here, we present an intensive spectroscopic campaign aimed to do so, which also serves as a valuable cross-check of the pulsar timing results.

## 2. OBSERVATIONS

Spectra of the counterpart of PSR J0337 were taken for us between 2012 November and 2013 January with the Gemini Multi Object Spectrograph (GMOS; Hook et al. 2004) of the Gemini-North telescope (see Table 1). We used the  $1200 \text{ line mm}^{-1}$  grating, covering the 3500–5000 Å range with the three  $2048 \times 4608$  pixel CCD detectors (which were binned  $4 \times 4$ , giving a spatial scale of  $0''.29 \text{ pix}^{-1}$  and a dispersion of  $0.94 \text{ Å pix}^{-1}$ ). As our object is relatively bright and has broad absorption lines, we could use poor-seeing conditions and hence opted for a wide,  $1''.5$  slit. With the typical seeing of  $1''.2$ , and given the anamorphic plate scale of  $0''.38 \text{ pix}^{-1}$  (for our grating setting; Murowinski et al. 2003), the resolution is  $\sim 3 \text{ Å}$ .

In each visit, we took two 10-minute exposures offset by  $50 \text{ Å}$  to cover the gaps between the detectors. Between the exposures, we took incandescent and CuAr lamp spectra for both settings, and before and after we took images through the slit to be able to constrain velocity offsets due to centering errors. For flux calibration, spectra were taken on a photometric night using the same settings through a  $5''$  slit, immediately followed by exposures of the white-dwarf spectrophotometric standard GD 71 (Bohlin & Gilliland 2004).

We oriented the slit to include another object on the slit, hoping to use it as a local flux and velocity reference. Unfortunately, the first object we picked – the only relatively bright one nearby, at a separation of  $27''.7$  and position angle  $8^{\circ}3$  – turned out to be a galaxy, which is not useful as it fills the slit. Hence, after the first set of data, we tried a another object (at  $58''$ ,  $-112^{\circ}$ ) which was fainter but which we hoped would have sufficiently narrow lines to still be useful. This, however, turned out to be a quasar. Hence, as will be clear below, our final velocity uncertainties have a significant component due to slit centroiding errors.

We reduced the data using custom python scripts. First, we subtracted bias levels as determined from over-scan regions for each of the six read-out channels, divided by their gains to give electron counts (with gains adjusted to ensure counts for flat fields were consistent between different read-out channels), combined detector halves, and divided by normalized flat fields. The spectra were extracted optimally, fitting at each dispersion

position the trace of the two objects with a Moffat function of the form  $(1 + [(x - x_c)/w]^2)^{-\beta}$  and the sky with a second-degree polynomial (with the trace position  $x_c$  and width  $w$  allowed to vary slowly with wavelength, and the exponent fixed to  $\beta = 2.5$ ).

For wavelength calibration, we first obtained accurate calibrations for a set of daytime CuAr spectra taken through a narrow,  $0''.5$  slit, in which many fewer lines are blended. Fitting a third-order polynomial for wavelength as a function of detector position, optimizing simultaneously for the offsets between the chips, we find root-mean-square residuals of  $0.017 \text{ Å}$  (for 79 lines; relative to copper and argon line wavelengths from the NIST database). For each nighttime arc, we measure the shift relative to the daytime arc taken at the same setting, and then apply the daytime calibration.

The spectra were flux-calibrated in three steps. First, all spectra were corrected approximately for atmospheric extinction using the average Mauna Kea extinction curve from Buton et al. (2013). Next, for the narrow-slit spectra, slit and cloud losses were measured by fitting a quadratic function to the count-rate ratio with the wide-slit observation. Finally, we divided by the instrumental response derived from the smoothed ratio of the count rates and fluxes of GD 71. While the wavelength region we covered does not fully overlap any of the photometric filters, extrapolating the short-wavelength part of the spectrum using a power-law gives a good agreement (better than  $1\text{-}\sigma$ ) with the measured SDSS  $u'$  photometry.

## 3. ANALYSIS

### 3.1. Velocities

We determined velocities by fitting a template to the data for a range of trial velocities, at each allowing for normalization and possible variations with wavelength using a linear function. For the template, we used a pure hydrogen model atmosphere with  $T_{\text{eff}} = 15,800 \text{ K}$  and  $\log_{10}(g) = 5.80$ , close to the best-fit parameters determined below (Section 3.2), convolving it with a Gaussian with a width set by the typical seeing of  $1''.2$  (equivalent to  $2.9 \text{ Å}$ ), and truncated at  $1''.5$  to mimic the slit. The fits to the spectra were good, with typical  $\chi^2 = 1440$  for 1527 degrees of freedom, and implied formal velocity uncertainties of  $\sim 4 \text{ km s}^{-1}$ .

An additional uncertainty in our velocities is the extent to which the object was properly centered in the slit. As mentioned, we had hoped to use a comparison star to calibrate this, but this turned out to be a quasar. Inspecting the images taken through the slit before and after the spectra, we find that the star has root-mean-square offsets from the slit center of  $0''.07$ , with the largest deviations about twice that (i.e., up to 2 unbinned pixels). The effect on velocity also depends on seeing (for very bad seeing, the slit is better filled and the effect minimized). From the acquisition images themselves, we find flux-weighted offsets about half as large, of  $0''.045$  (rms). The shifts for the spectra are slightly smaller, since the traces in the spectra show slightly larger seeing, presumably because of jitter in the telescope pointing. Using the centroiding positions from the acquisition images combined with the seeing from the spectral traces, we infer flux-weighted offsets of  $0''.034$  (rms), corresponding to wavelength shifts of  $0.060 \text{ Å}$  and, for an assumed effective

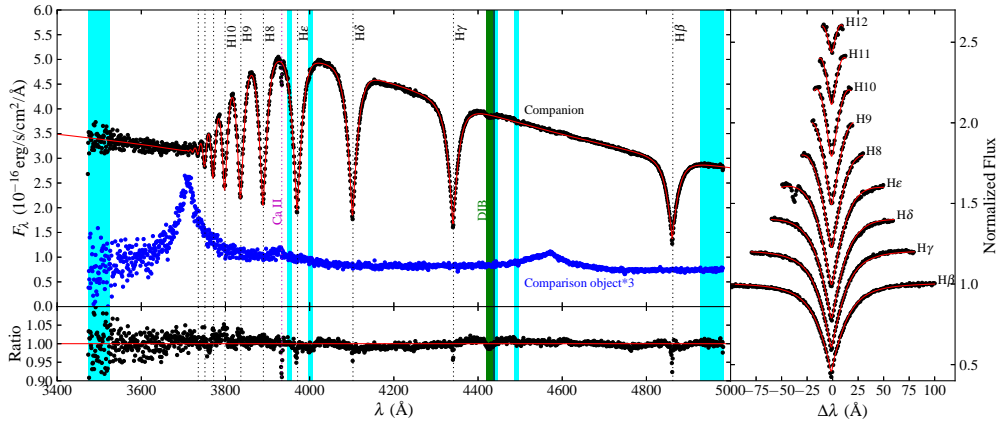


**Figure 1.** Left: Composite spectrum of the optical counterpart to PSR J0337. The individual spectra have been shifted by their measured velocities and summed. Overdrawn is the best-fit model atmosphere (red), with effective temperature 15,800 K and surface gravity  $\log(g) = 5.82$ . We also show the comparison source below the counterpart (multiplied by 3 for clarity), which we identified as a  $z = 1.4$  quasar: the broad emission line at  $3717 \text{ \AA}$  is C IV  $\lambda 1549$ . The vertical lines mark the Balmer series, with Ca II  $\lambda 3933$  also labeled. The cyan bands show where we have data from only half of the spectra, either because of the chip gaps or the ends of the spectral coverage. The green band shows the diffuse interstellar band (DIB) at  $4430 \text{ \AA}$ . Right: fits to the individual Balmer lines (as labeled), with the model overdrawn in red. Bottom: the ratio of the counterpart spectrum with respect to the model: small deviations are seen at some of the lower-order Balmer lines, with a more significant deviation at the Ca II  $\lambda 3933$  line.

wavelength of  $4200 \text{ \AA}$ , velocity shifts of  $\sim 4.3 \text{ km s}^{-1}$ . In Table 1, we list the velocities corrected for these shifts and corrected to the Solar System barycenter.

To determine the orbit, we fit the velocities to a model  $v_{\text{WD}}(t) = \gamma - (1/q_I) \times v_{\text{PSR}}^{\text{in}}(t) + v_{\text{PSR}}^{\text{out}}(t)$ , where  $\gamma$  is the systemic radial velocity,  $q_I \equiv M_{\text{WD}}/M_{\text{PSR}}$  is the inner mass ratio,  $v_{\text{PSR}}^{\text{in}}$  is the radial velocity of the pulsar in the inner orbit, and  $v_{\text{PSR}}^{\text{out}}$  is the radial velocity of the inner-orbit barycenter in the outer orbit, both as inferred from the timing model (with radial-velocity amplitudes  $K_{\text{PSR}}^{\text{in}} = 16.291$  and  $K_{\text{PSR}}^{\text{out}} = 4.978 \text{ km s}^{-1}$ , respectively). Such a model is traditional for pulsar binaries, where the period and pulsar’s velocity are known but the mass ratio is not. For PSR J0337, we do know  $q_I$ , but the analysis serves as a valuable check of the full timing model. The velocities fit reasonably well (Figure 2), although the fit is formally unacceptable, with  $\chi^2 = 55.9$  for 33 degrees of freedom (35 spectra, 2 parameters), likely because of remaining uncertainties in the slit centering (e.g., due to differential atmospheric refraction). In order to account for this in our parameter uncertainties, we added an additional uncertainty of  $3.3 \text{ km s}^{-1}$  to the velocity errors (in quadrature), giving a reduced  $\chi^2$  of 1.0. With that, we find  $\gamma = 29.7 \pm 0.9 \text{ km s}^{-1}$  and  $q_I = 0.1364 \pm 0.0015$ , implying  $K_{\text{WD}}^{\text{in}} = 119.4 \pm 1.3 \text{ km s}^{-1}$ . This is fully consistent with the value measured from pulsar timing (Ransom et al. 2014):  $q_I = 0.13737 \pm 0.00004$ .

For completeness, we note that our results do not depend on whether we include the centroiding shifts, although the fit becomes substantially worse if we do not ( $\chi^2 = 115$ ). The fit also does not depend on whether we took the centroid from the nearest acquisition image, or rather interpolated between images taken before and after the spectra. Furthermore, if we leave the prefactor for the centroiding shift free, i.e., include an additional term  $\alpha \Delta v$  in the fit, we find  $\alpha = 1.13 \pm 0.16$ . Finally, if we ignore the contribution from the outer orbit, we find  $\chi^2 = 58.5$ , i.e., the outer orbit is detected marginally even in our velocities.

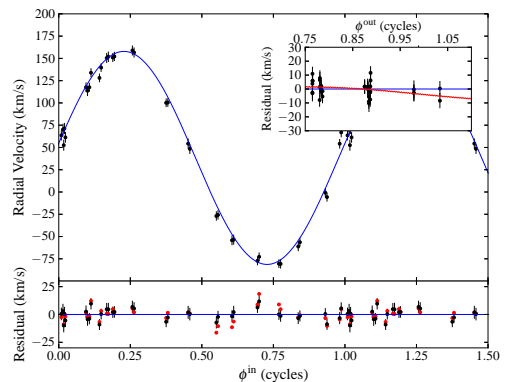


**Figure 2.** Radial velocities of the optical counterpart to PSR J0337. *Main panel:* Observed velocities plus the velocity expected for the outer orbit, as a function of the phase of the inner orbit (repeated 1.5 times for clarity), with the best-fit model overdrawn (solid line). *Lower panel:* Residuals with respect to that model with and without correction for small slit-centering errors (black and red points, respectively). *Inset:* Residuals as a function of outer orbital phase, with inner velocity contribution removed, and with models with and without the outer object overdrawn (blue and red solid lines, respectively).

### 3.2. Model atmosphere fits

Given the velocities determined above, we created a composite summed spectrum (Figure 1) by shifting each of the individual measurements back to zero velocity. We see strong Balmer lines, as well as a weaker Ca II  $\lambda 3933$  absorption line and some broad absorption near  $4430 \text{ \AA}$  associated with a diffuse interstellar band (DIB).

Metal lines are occasionally seen from white dwarfs (Gänsicke et al. 2012), especially those with low gravities ( $< 5.6$ ; Kilic et al. 2012; Kaplan et al. 2013), and they are commonly interpreted as signs of accretion. However, Ca II absorption can also be interstellar in origin. We compared the velocity centroid and width of the Ca II line using both the spectra corrected for the motion of the white dwarf and only corrected for the motion of the

Earth around the Solar System barycenter. We find that the line is marginally narrower when not correcting for the motion of the white dwarf (the depth increases from  $9.3 \pm 0.6\%$  to  $10.2 \pm 0.6\%$ ), suggesting that it is interstellar in this case. This is confirmed by a line of similar strength that we see in the spectrum of the comparison quasar, although the signal-to-noise is lower. The centroid of the Ca II line as determined from the uncorrected data is  $44 \pm 6 \text{ km s}^{-1}$ , implying a systemic radial velocity of the pulsar relative to the interstellar medium of  $-14 \pm 6 \text{ km s}^{-1}$ ; this is not very different from the expectations using the Brand & Blitz (1993) rotation curve for a distance of 1.3 kpc (see below), where the radial velocity goes between 0 and  $-4 \text{ km s}^{-1}$  along the line-of-sight. Similarly, with data only corrected for the Earth’s motion (and excluding data where the gap between the green and red CCDs came near the DIBs), we measure a depth at the center of the DIB of  $2.0 \pm 0.2\%$ . Based on the empirical relation of Krelowski et al. (1987), we infer an extinction  $A_V \approx 0.3 \text{ mag}$ .

We next fit for the atmospheric parameters for the white dwarf by comparing against pure hydrogen models computed by one of us (D. Koester). These models covered  $T_{\text{eff}} = 15,500 \text{ K}$  to  $16,500 \text{ K}$  in steps of  $100 \text{ K}$  and  $\log_{10}(g) = 5.50$  to  $6.50$  in steps of  $0.1 \text{ dex}$ . We identified some line-free regions to fit a cubic polynomial that represented the difference in normalization between the models and the data, and computed the  $\chi^2$  of each model with respect to the data. The models were convolved with a function to represent the slit and the average seeing ( $1''.2$ ), as discussed above. We excluded the region around the Ca II  $\lambda 3933$  line and He (which is blended with Ca II  $\lambda 3968$ ). Overall, our initial fit has  $T_{\text{eff}} = 15,780 \text{ K}$  and  $\log_{10}(g) = 5.82$ . This fit has  $\chi^2 = 4098.2$  for 1613 degrees-of-freedom, so it is formally unacceptable. Much of the deviation comes from the cores of the lower-order Balmer lines (Figure 1, lower panel). These deviations might be indicative of the outer member of the binary (i.e., third light). However, we find that they track the white dwarf’s orbit, so are likely just errors in our model or calibration. In particular, NLTE effects might be important; in higher-gravity white dwarfs, they cause deeper cores for H $\alpha$  and H $\beta$  at these temperatures.

Computing the best-fit model for each individual observation gave similar results, with  $T_{\text{eff}} = 15,882 \pm 35 \text{ K}$  and  $\log_{10}(g) = 5.85 \pm 0.01$ , where the uncertainties are the formal errors in the means. To account for the formally poor fit and model uncertainties, we increase the uncertainties to  $\pm 0.05 \text{ dex}$  and  $\pm 100 \text{ K}$ , which are about the smallest we would believe for an object in this relatively unconstrained part of the white dwarf cooling sequence. We therefore adopt as our best-fit model  $T_{\text{eff}} = 15,800 \pm 100 \text{ K}$  and  $\log_{10}(g) = 5.82 \pm 0.05$ . For this effective temperature, the best-fit extinction based on the photometry is  $A_V = 0.44 \pm 0.04 \text{ mag}$  (Ransom et al. 2014).

#### 4. DISCUSSION & CONCLUSIONS

Our measurements provide the velocities and atmospheric parameters of the inner white dwarf in the PSR J0337 system. The velocities serve to confirm the more precise ones inferred from pulsar timing. In addition, they show that the systemic velocity is low. This

is not unexpected, since any kick imparted to the system in the supernova explosion that formed the neutron star must have been small for the triple to survive (Tauris & van den Heuvel 2014). One thus expects the proper motion to be similarly small.

Our measurement of the surface gravity, combined with the precise mass from timing, implies a radius of  $0.091 \pm 0.005 R_{\odot}$ . Combining this in turn with the effective temperature, extinction, and photometry, one infers a distance of  $1300 \pm 80 \text{ pc}$  (Ransom et al. 2014). With an accurate parallax from very-long baseline interferometry (measurements are in progress), this can be used to infer the surface gravity and thus test the model atmospheres in an otherwise poorly constrained regime.

The mass and radius of the inner white dwarf are consistent with those expected for a young, low-mass helium-core white dwarf, similar to the white dwarf companions found in other binaries (Section 1). Compared to low-mass white dwarfs around pulsars,<sup>11</sup> however, the source stands out for being hotter than most. This must be intrinsic as possible contributions from pulsar irradiation and tidal heating are negligible.

The high temperature is surprising as it would suggest the system is in a short-lived state and hence that similar systems are common – which, empirically, they are not. This suggestion arises because in current evolutionary models of helium white dwarfs, temperatures in excess of  $\sim 12,000 \text{ K}$  are only achieved in models with unstable shell flashes (e.g., Driebe et al. 1998; Althaus, Serenelli, & Benvenuto 2001). In those shell flashes, however, most of the thick hydrogen layer is lost, and hence the white dwarf will cool relatively quickly. Furthermore, while the flashing state may last  $\sim 200 \text{ Myr}$  (Althaus et al. 2013), the typical cooling timescales at these temperatures are short, a few  $10 \text{ Myr}$  for each flash, and hence the total time spent at high temperatures is often  $< 100 \text{ Myr}$ , depending on mass. These timescales are still far longer than the expected sedimentation timescale for helium ( $\sim 10^3 \text{ yr}$ ) following mixing during a shell flash, consistent with the lack of any He I in the spectrum of the inner WD (cf. Kaplan et al. 2013). Based on inspection, we can roughly limit its abundance to  $10^{-2.5} \text{ H}$  (by number), which would not change our inferred  $\log_{10}(g)$  by more than our quoted uncertainty. If the inner white dwarf is really only a few  $100 \text{ Myr}$  old, it almost certainly formed last, as also expected from simple models (Ransom et al. 2014; Tauris & van den Heuvel 2014), although we cannot strictly exclude the opposite: at the upper limit to the temperature of the outer WD of  $20,000 \text{ K}$  (Ransom et al. 2014), the cooling time would be  $30\text{--}100 \text{ Myr}$ .

Of course, it could be a coincidence that we found such a hot white-dwarf companion. However, a similarly hot companion was found for PSR J1816+4510 (Kaplan et al. 2013). Since typical millisecond pulsars remain visible for a Hubble time, and since we know  $\sim 50$  pulsars with low-mass white dwarf companions, this suggests that white dwarfs can stay hot for  $\sim 500 \text{ Myr}$ ,

<sup>11</sup> One cannot easily compare low-mass white dwarfs with white-dwarf or A-star companions, since for those systems there are strong observational biases to find hotter, more luminous and larger white dwarfs.

substantially longer than expected in current theoretical models. The discrepancy is made worse by the fact that white dwarfs with mass below  $\lesssim 0.18 M_{\odot}$  are not expected to get this hot at all (they should not have flashes). Observationally, however, lifetimes of a few hundred Myr seem also indicated by the prevalence of hot, low-mass white dwarfs around A stars (which have ages of  $\lesssim 1$  Gyr).

We thank an anonymous referee for a helpful suggestion. We thank Gemini staff Atsuko Nitta, John Blakeslee, and Kristin Chiboucas for helping assure the high quality of these data. The National Radio Astronomy Observatory is a facility of the National Science Foundation, operated under cooperative agreement by Associated Universities, Inc. Balmer/Lyman lines in the models were calculated with the modified Stark broadening profiles of Tremblay & Bergeron (2009), kindly made available by the authors. M.H.v.K. and I.H.S. acknowledge funding from NSERC Discovery Grants. J.W.T.H. and A.M.A. acknowledge support from a Vrije Competitie grant from NWO. We made extensive use of SIMBAD, ADS, and Astropy (<http://www.astropy.org>; Astropy Collaboration et al. 2013).

*Facilities:* Gemini:Gillett (GMOS)

#### REFERENCES

- Alberts, F., Savonije, G. J., van den Heuvel, E. P. J., & Pols, O. R. 1996, *Nature*, 380, 676
- Althaus, L. G., Córscico, A. H., Isern, J., & García-Berro, E. 2010, *A&A Rev.*, 18, 471
- Althaus, L. G., Miller Bertolami, M. M., & Córscico, A. H. 2013, *A&A*, 557, A19
- Althaus, L. G., Serenelli, A. M., & Benvenuto, O. G. 2001, *MNRAS*, 323, 471
- Antoniadis, J., et al. 2013, *Science*, 340, 448
- Antoniadis, J., van Kerkwijk, M. H., Koester, D., Freire, P. C. C., Wex, N., Tauris, T. M., Kramer, M., & Bassa, C. G. 2012, *MNRAS*, 423, 3316
- Astropy Collaboration, et al. 2013, *A&A*, 558, A33
- Bedin, L. R., Salaris, M., Piotto, G., King, I. R., Anderson, J., Cassisi, S., & Momany, Y. 2005, *ApJ*, 624, L45
- Bohlin, R. C. & Gilliland, R. L. 2004, *AJ*, 128, 3053
- Boyles, J., et al. 2013, *ApJ*, 763, 80
- Brand, J. & Blitz, L. 1993, *A&A*, 275, 67
- Brown, W. R., Kilic, M., Allende Prieto, C., Gianninas, A., & Kenyon, S. J. 2013, *ApJ*, 769, 66
- Buton, C., et al. 2013, *A&A*, 549, A8
- D’Antona, F., Ventura, P., Burderi, L., & Teodorescu, A. 2006, *ApJ*, 653, 1429
- Deloye, C. J. & Bildsten, L. 2003, *ApJ*, 598, 1217
- Driebe, T., Schoenberner, D., Bloeker, T., & Herwig, F. 1998, *A&A*, 339, 123
- Gänsicke, B. T., Koester, D., Farihi, J., Girven, J., Parsons, S. G., & Breedt, E. 2012, *MNRAS*, 424, 333
- Hook, I. M., Jørgensen, I., Allington-Smith, J. R., Davies, R. L., Metcalfe, N., Murowinski, R. G., & Crampton, D. 2004, *PASP*, 116, 425
- Iben, Jr., I. & Livio, M. 1993, *PASP*, 105, 1373
- Iben, Jr., I. & Tutukov, A. V. 1984, *ApJS*, 54, 335
- Kaplan, D. L., Bhalariao, V. B., van Kerkwijk, M. H., Koester, D., Kulkarni, S. R., & Stovall, K. 2013, *ApJ*, 765, 158
- Kaplan, D. L., Bildsten, L., & Steinfadt, J. D. R. 2012, *ApJ*, 758, 64
- Kilic, M., Brown, W. R., Allende Prieto, C., Kenyon, S. J., Heinke, C. O., Agüeros, M. A., & Kleinman, S. J. 2012, *ApJ*, 751, 141
- Krelowski, J., Walker, G. A. H., Grieve, G. R., & Hill, G. M. 1987, *ApJ*, 316, 449
- Lorimer, D. R., Lyne, A. G., Festin, L., & Nicastro, L. 1995, *Nature*, 376, 393
- Lynch, R. S., et al. 2013, *ApJ*, 763, 81
- Marsh, T. R., Dhillion, V. S., & Duck, S. R. 1995, *MNRAS*, 275, 828
- Marsh, T. R., Nelemans, G., & Steeghs, D. 2004, *MNRAS*, 350, 113
- Murowinski, R. G., et al. 2003, in *Society of Photo-Optical Instrumentation Engineers (SPIE) Conference Series*, Vol. 4841, ed. M. Iye & A. F. M. Moorwood, 1189–1200
- Panei, J. A., Althaus, L. G., Chen, X., & Han, Z. 2007, *MNRAS*, 382, 779
- Ransom, S. M., et al. 2014, *Nature*, 505, 520
- Serenelli, A. M., Althaus, L. G., Rohrmann, R. D., & Benvenuto, O. G. 2002, *MNRAS*, 337, 1091
- Tauris, T. M., Langer, N., & Kramer, M. 2012, *MNRAS*, 425, 1601
- Tauris, T. M. & van den Heuvel, E. P. J. 2014, *ApJ*, in press
- Tremblay, P.-E. & Bergeron, P. 2009, *ApJ*, 696, 1755
- van Kerkwijk, M. H., Bassa, C. G., Jacoby, B. A., & Jonker, P. G. 2005, in *ASP Conf. Ser.*, Vol. 328, *Binary Radio Pulsars*, ed. F. A. Rasio & I. H. Stairs (San Francisco, CA: ASP), 357, arXiv:astro-ph/0405283
- van Kerkwijk, M. H., Bergeron, P., & Kulkarni, S. R. 1996, *ApJ*, 467, L89
- Webbink, R. F. 1984, *ApJ*, 277, 355

**Table 1**  
Log of observations and velocity measurements

Date None	UT None	$\lambda_c^a$ (Å)	Seeing (arcsec)	Shift <sup>b</sup> (arcsec)	Offset <sup>c</sup> (arcsec)	MJD <sub>bar</sub> None	$\phi^{\text{in,d}}$ None	$v_{\text{PSR}}^{\text{in,e}}$ (km s <sup>-1</sup> )	$v_{\text{PSR}}^{\text{out,f}}$ (km s <sup>-1</sup> )	$v_{\text{WD}}^g$ (km s <sup>-1</sup> )
2012 Nov 09...	08:44	4250	1.4	-0.024	-0.010	56240.3674	0.0918	-10.68	4.92	117 ± 4
	08:56	4200	1.3	-0.055	-0.025	56240.3760	0.0971	-11.09	4.92	112 ± 5
	09:10	4250	1.3	-0.055	-0.025	56240.3863	0.1034	-11.55	4.92	117 ± 4
	09:24	4200	1.2	-0.057	-0.029	56240.3956	0.1091	-11.96	4.92	133 ± 4
	11:32	4250	1.9	0.034	0.009	56240.4850	0.1640	-15.00	4.92	149 ± 4
	11:46	4200	1.9	0.036	0.009	56240.4945	0.1698	-15.22	4.92	149 ± 5
2012 Nov 14...	07:52	4250	1.0	-0.047	-0.028	56245.3318	0.1387	-13.79	4.84	128 ± 4
	08:06	4200	0.9	-0.047	-0.030	56245.3413	0.1445	-14.10	4.84	139 ± 4
	12:22	4250	1.8	-0.021	-0.006	56245.5193	0.2537	-16.08	4.84	159 ± 5
	12:36	4200	1.8	0.017	0.005	56245.5288	0.2596	-15.98	4.84	155 ± 5
2012 Nov 15...	08:23	4250	1.2	-0.133	-0.067	56246.3536	0.7658	15.85	4.82	-81 ± 4
	08:37	4200	1.5	-0.131	-0.050	56246.3632	0.7717	15.70	4.82	-81 ± 4
	11:02	4250	1.6	-0.060	-0.021	56246.4636	0.8333	12.89	4.82	-61 ± 4
	11:15	4200	1.5	-0.050	-0.020	56246.4731	0.8392	12.51	4.82	-57 ± 4
2012 Nov 16...	08:05	4250	0.8	-0.045	-0.034	56247.3409	0.3718	-10.11	4.79	100 ± 4
	08:19	4200	0.8	-0.052	-0.039	56247.3505	0.3776	-9.63	4.79	100 ± 4
2012 Dec 15...	08:45	4250	1.3	-0.065	-0.030	56276.3683	0.1858	-15.72	3.33	150 ± 4
	08:58	4200	1.3	-0.027	-0.013	56276.3772	0.1912	-15.86	3.32	151 ± 4
2012 Dec 17...	10:09	4250	2.2	-0.051	-0.011	56278.4272	0.4491	-2.93	3.17	54 ± 5
	10:23	4200	2.1	-0.078	-0.018	56278.4367	0.4550	-2.34	3.17	47 ± 5
2012 Dec 18...	04:54	4250	1.2	0.011	0.005	56279.2084	0.9285	4.98	3.11	-1 ± 4
	05:08	4200	1.2	-0.013	-0.006	56279.2180	0.9343	4.41	3.11	-6 ± 4
	08:16	4250	2.4	-0.115	-0.021	56279.3484	0.0144	-3.71	3.10	52 ± 5
	08:29	4200	2.2	-0.177	-0.036	56279.3580	0.0202	-4.29	3.10	60 ± 5
2012 Dec 19...	05:07	4250	1.2	0.075	0.036	56280.2176	0.5477	6.92	3.03	-27 ± 4
	05:21	4200	1.3	0.070	0.032	56280.2272	0.5535	7.46	3.03	-26 ± 4
	07:16	4250	1.6	0.114	0.041	56280.3068	0.6024	11.48	3.02	-55 ± 4
	07:30	4200	1.9	0.119	0.033	56280.3164	0.6083	11.90	3.02	-55 ± 5
	10:45	4250	1.1	-0.054	-0.030	56280.4519	0.6914	15.86	3.01	-78 ± 4
	10:58	4200	1.0	-0.089	-0.054	56280.4614	0.6973	15.99	3.01	-74 ± 3
2013 Jan 18...	07:33	4250	1.3	0.004	0.002	56310.3181	0.0074	-4.34	0.19	63 ± 5
	07:46	4200	1.5	-0.032	-0.012	56310.3272	0.0130	-4.88	0.19	69 ± 6
	07:58	4200	1.5	-0.032	-0.012	56310.3357	0.0182	-5.38	0.19	70 ± 5
2013 Feb 05...	05:33	4250	1.6	-0.025	-0.008	56328.2349	0.9810	-3.92	-1.61	55 ± 4
	05:46	4200	1.6	-0.030	-0.010	56328.2438	0.9864	-4.45	-1.62	67 ± 4

<sup>a</sup> Center wavelength of each observation.

<sup>b</sup> Deviation of the target from the center of the slit in the acquisition image.

<sup>c</sup> Deviation of the center of light from the center of the slit, calculated using the FWHM measured from the spectra.

<sup>d</sup> Orbital phase for the inner orbit.

<sup>e</sup> Inferred velocity for the pulsar due to the inner orbit relative to the system barycenter.

<sup>f</sup> Inferred velocity for the pulsar due to the outer orbit relative to the system barycenter

<sup>g</sup> Measured velocity for the white dwarf, with all corrections applied.